# Experimentelle Methoden der Teilchenphysik

## Sommersemester 2011/2012

## Albert-Ludwigs-Universität Freiburg


Prof. Markus Schumacher

Physikalisches Institut, Westbau, 2. OG Raum 008

Telefon 07621 203 7612

E-Mail: Markus.Schumacher@physik.uni-freiburg.de

Kapitel 4: Gasgefüllte Ionisationsdetektoren

http://terascale.physik.uni-freiburg.de/lehre/Sommersemester%202012

# Materialwerte zur Ionisiationsausbeute

| Gas | Dichte ρ [g/cm$^3$] | $I_0$ [eV] | W [eV] | $n_p$ [cm$^{-1}$] | $n_T$ [cm$^{-1}$] |
|---|---|---|---|---|---|
| $H_2$ | 8.99 x 10$^{-5}$ | 15.4 | 37 | 5.2 | 9.2 |
| He | 1.78 x 10$^{-4}$ | 24.6 | 41 | 5.9 | 7.8 |
| $N_2$ | 1.23 x 10$^{-3}$ | 15.5 | 35 | 10 | 56 |
| $O_2$ | 1.43 x 10$^{-3}$ | 12.2 | 31 | 22 | 73 |
| Ne | 9.00 x 10$^{-4}$ | 21.6 | 36 | 12 | 39 |
| Ar | 1.78 x 10$^{-3}$ | 15.8 | 26 | 29 | 94 |
| Kr | 3.74 x 10$^{-3}$ | 14.0 | 24 | 22 | 192 |
| Xe | 5.89 x 10$^{-3}$ | 12.1 | 22 | 44 | 307 |
| $CO_2$ | 1.98 x 10$^{-3}$ | 13.7 | 33 | 34 | 91 |
| $CH_4$ | 7.17 x 10$^{-4}$ | 13.1 | 28 | 16 | 53 |
| $C_4H_{10}$ | 2.67 10-3 | 10.8 | 23 | 46 | 195 |

mittl. Ionisationspot. / Hüllenelek.
mitterer Energieverl./Ionenpaar
Anzahl Primär Elektron-Ion Paare
Totale Anzahl Elektron-Ion Paare

Totale Anzahl der erzeugten Elektron-Ion

Paare: $n_T = \frac{\Delta E}{W_i} = \frac{\frac{dE}{dx}\Delta x}{W_i}$ mit

- $\Delta E$ = totaler Energieverlust in $\Delta x$ und
- $W_i$ = mittlerer Energieverlust pro **erzeugtes** Ionenpaar: $n_T \approx 2 \ldots 7 \cdot n_p$

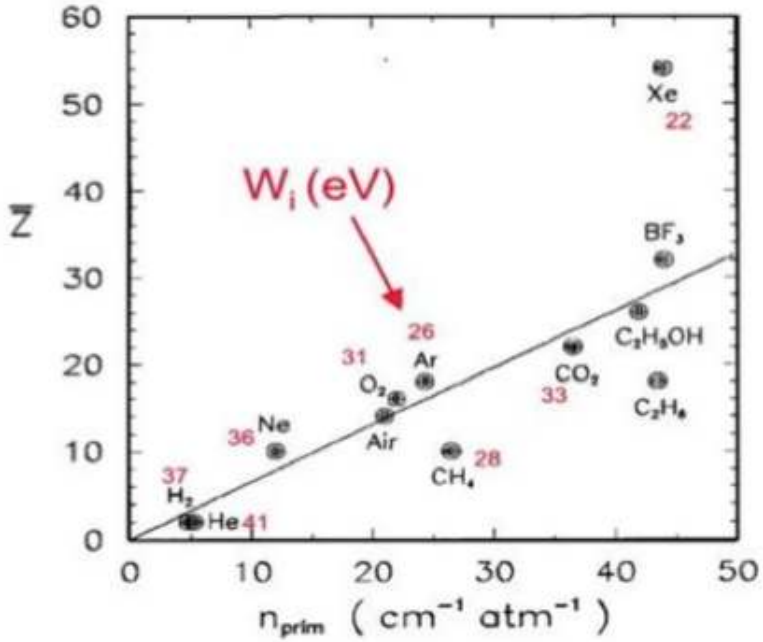

# Materialwerte zur Ionisiationsausbeute

**Table 28.5:** Properties of noble and molecular gases at normal temperature and pressure (NTP: 20° C, one atm). $E_X$, $E_I$: first excitation, ionization energy; $W_I$: average energy per ion pair; $dE/dx|_{\min}$, $N_P$, $N_T$: differential energy loss, primary and total number of electron-ion pairs per cm, for unit charge minimum ionizing particles.

| Gas | Density, $\mathrm{mg\,cm^{-3}}$ | $E_x$ eV | $E_I$ eV | $W_I$ eV | $dE/dx\|_{\min}$ $\mathrm{keV\,cm^{-1}}$ | $N_P$ $\mathrm{cm^{-1}}$ | $N_T$ $\mathrm{cm^{-1}}$ |
|---|---|---|---|---|---|---|---|
| He | 0.179 | 19.8 | 24.6 | 41.3 | 0.32 | 3.5 | 8 |
| Ne | 0.839 | 16.7 | 21.6 | 37 | 1.45 | 13 | 40 |
| Ar | 1.66 | 11.6 | 15.7 | 26 | 2.53 | 25 | 97 |
| Xe | 5.495 | 8.4 | 12.1 | 22 | 6.87 | 41 | 312 |
| $CH_4$ | 0.667 | 8.8 | 12.6 | 30 | 1.61 | 28 | 54 |
| $C_2H_6$ | 1.26 | 8.2 | 11.5 | 26 | 2.91 | 48 | 112 |
| $iC_4H_{10}$ | 2.49 | 6.5 | 10.6 | 26 | 5.67 | 90 | 220 |
| $CO_2$ | 1.84 | 7.0 | 13.8 | 34 | 3.35 | 35 | 100 |
| $CF_4$ | 3.78 | 10.0 | 16.0 | 54 | 6.38 | 63 | 120 |

# Beweglichkeit und Diffusion von Ionen

Table 1.6. *Average mean free path $\lambda_{ion}$, diffusion constant $D_{ion}$ and mobilities $\mu_{ion}$ of ions in some gases for standard pressure and temperature [32, 71]*

| Gas | $\lambda_{ion}$ [cm] | $D_{ion}$ [cm$^2$/s] | $\mu_{ion}$ $\left[\frac{\text{cm/s}}{\text{V/cm}}\right]$ |
|---|---|---|---|
| $H_2$ | $1.8 \cdot 10^{-5}$ | 0.34 | 13.0 |
| He | $2.8 \cdot 10^{-5}$ | 0.26 | 10.2 |
| Ar | $1.0 \cdot 10^{-5}$ | 0.04 | 1.7 |
| $O_2$ | $1.0 \cdot 10^{-5}$ | 0.06 | 2.2 |

# Driftgeschwindigkeit und Diffusionkoeffizienten

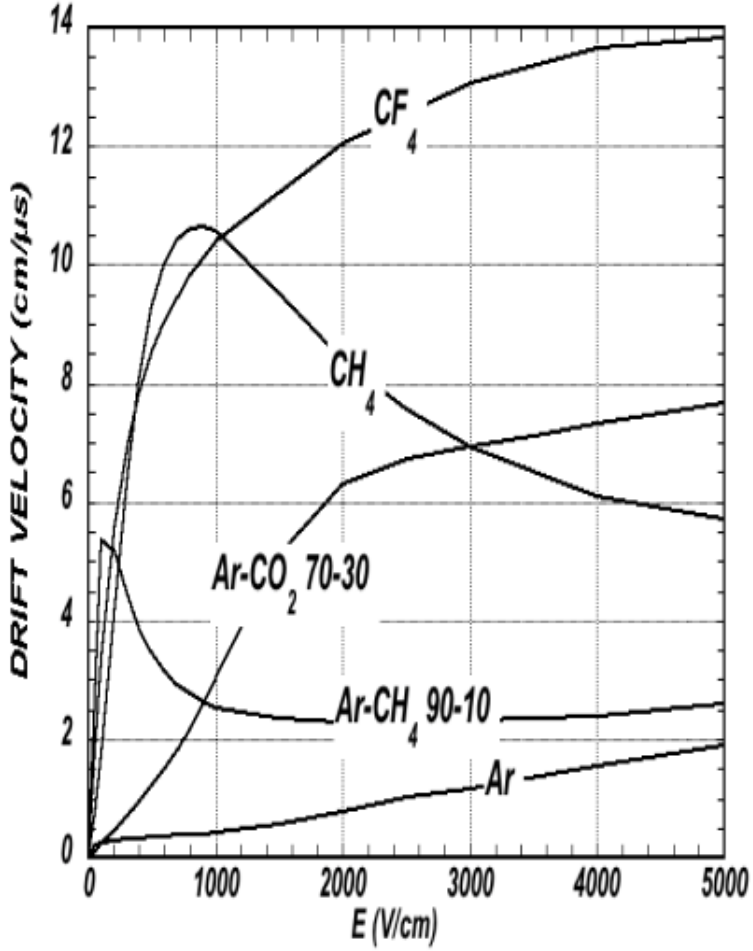


Figure 28.4: Computed electron drift velocity as a function of electric field in several gases at NTP and $B = 0$ [65].

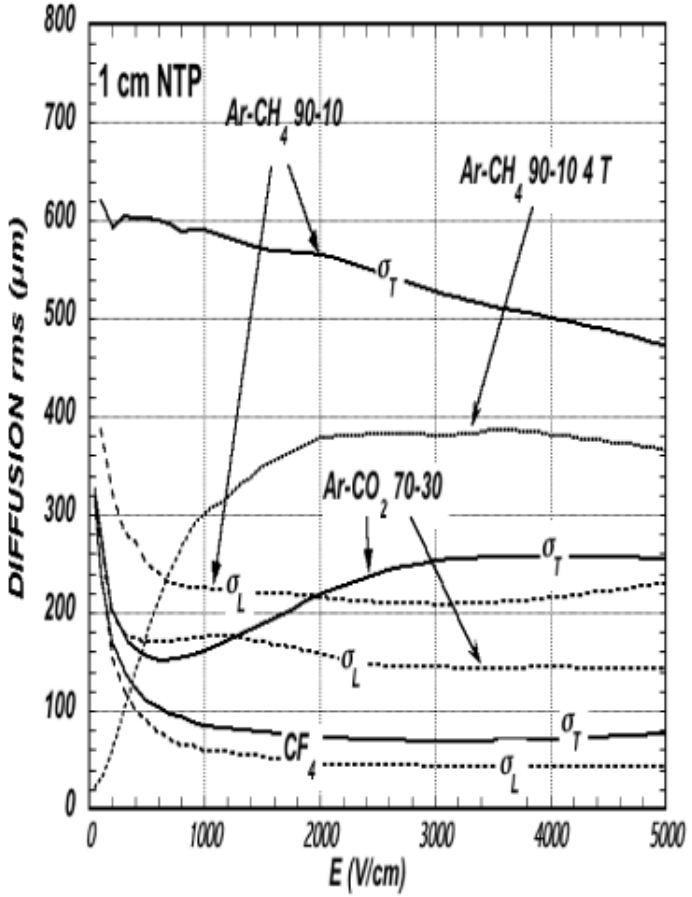


Figure 28.5: Electron longitudinal diffusion ($\sigma_L$) (dashed lines) and transverse diffusion ($\sigma_T$) (full lines) for 1 cm of drift at NTP and $B = 0$. The dotted line shows $\sigma_T$ for the P10 mixture at 4 T [65].

# Driftgeschwindigkeit von Gasgemischen

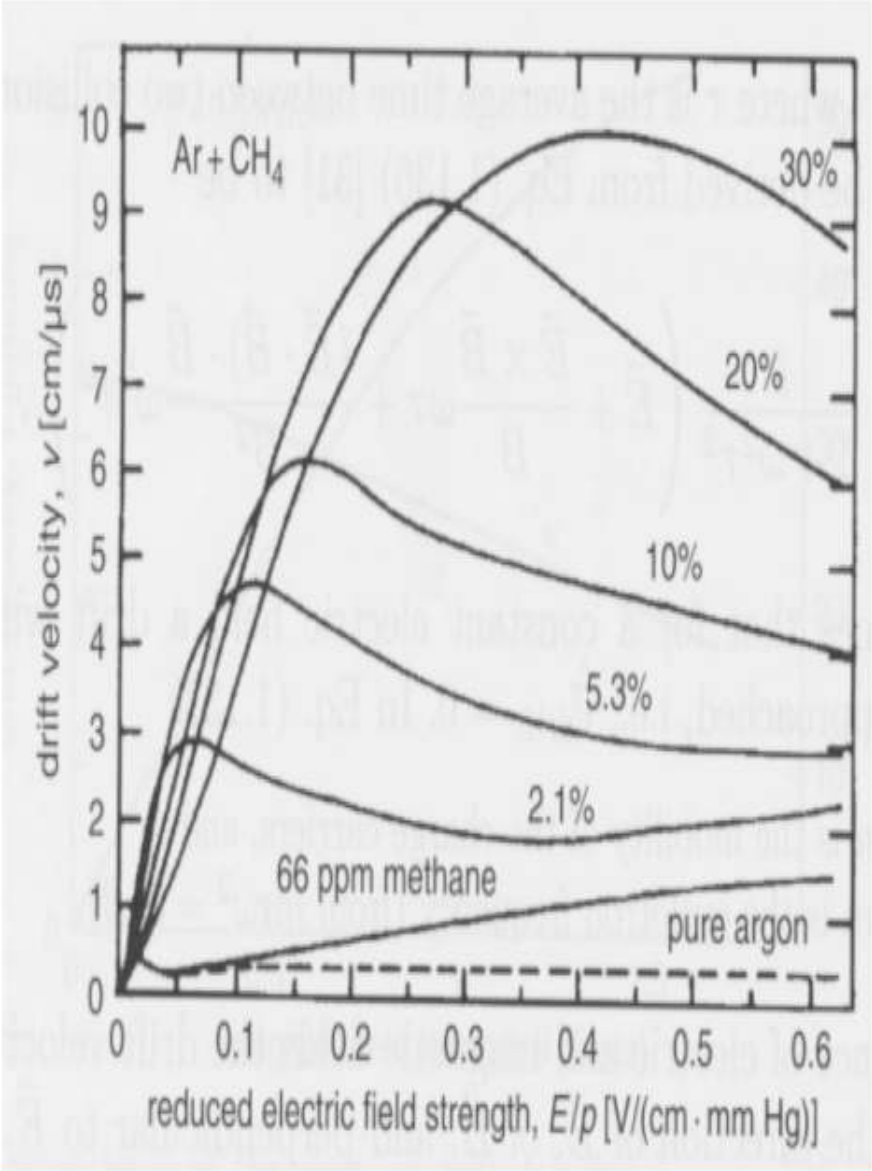


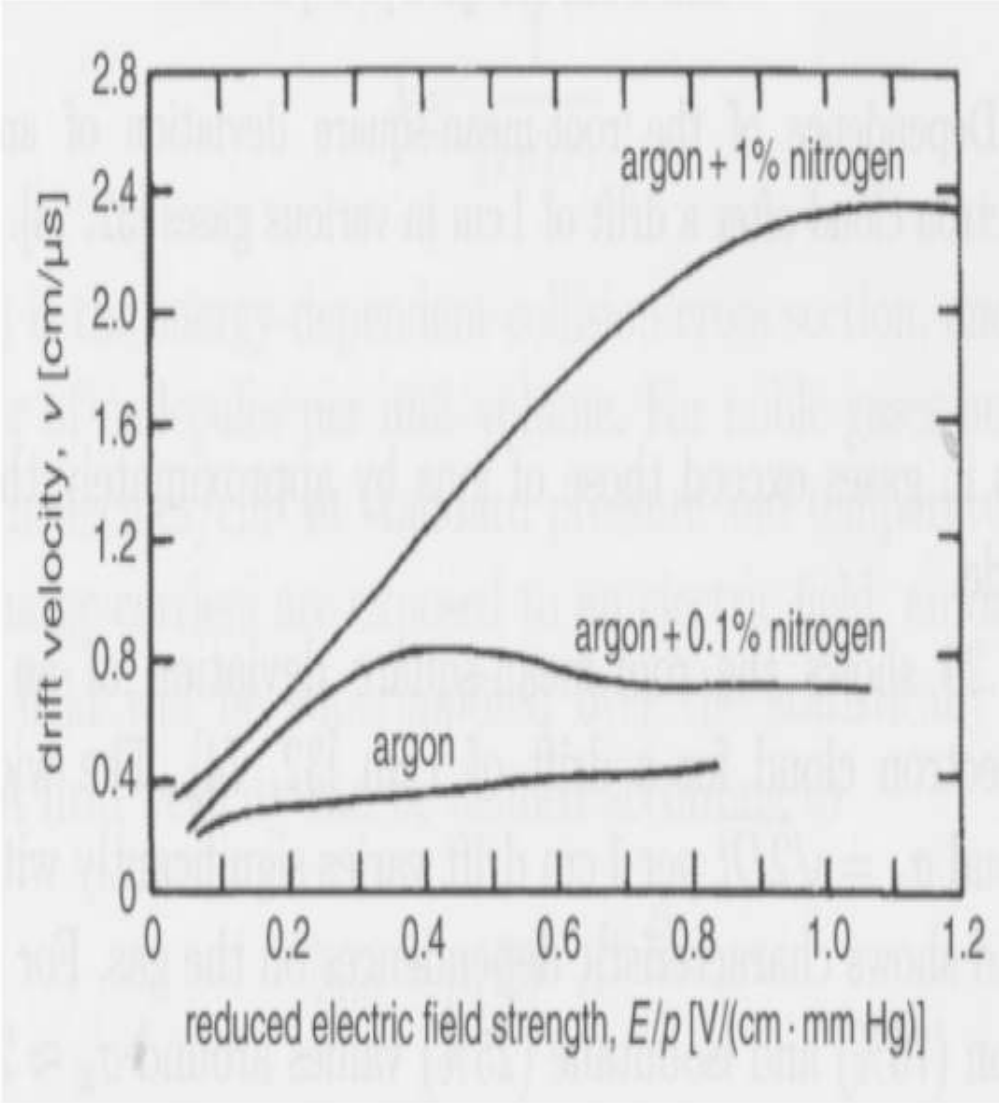

# Driftgeschwindigkeit und Lorentzwinkel im B-Feld

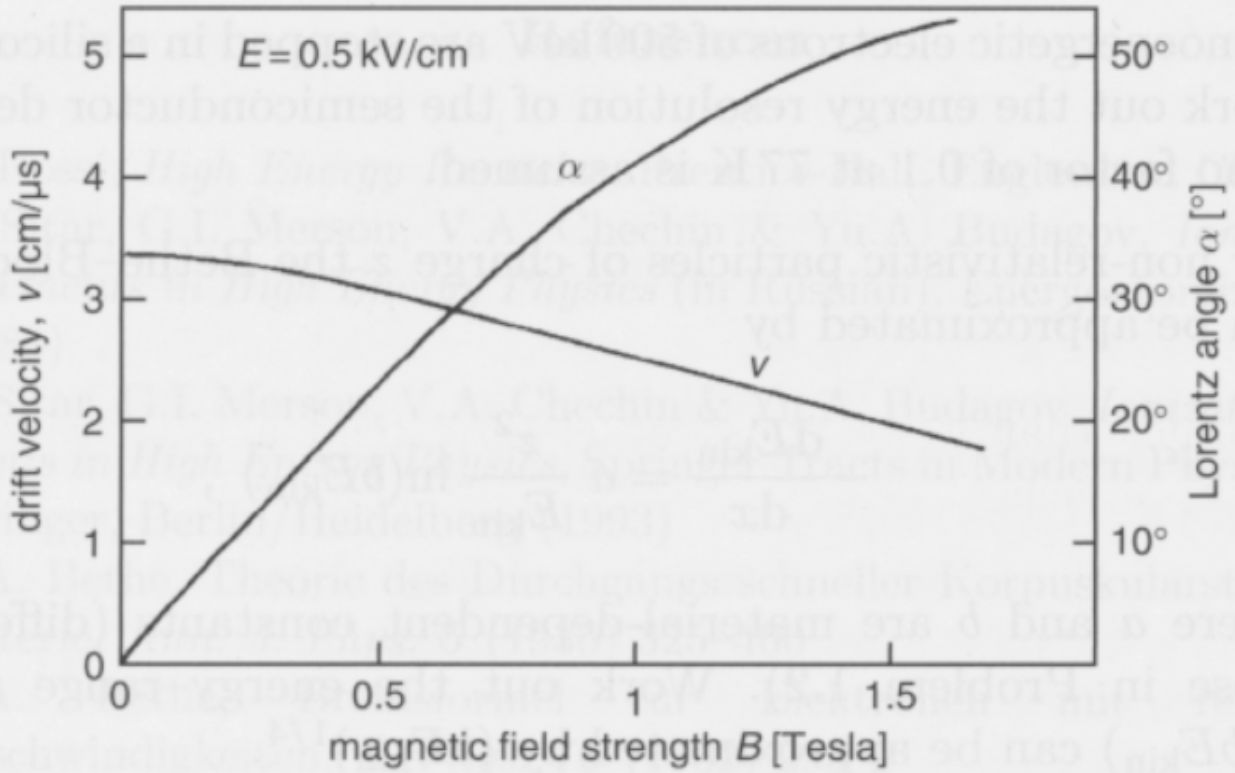


Fig. 1.25. Dependence of the electron drift velocity $\vec{v}_{\text{drift}}$ and the Lorentz angle $\alpha$ on the magnetic field for low electric field strengths (500 V/cm) in a gas mixture of argon (67.2%), isobutane (30.3%) and methylal (2.5%) [32, 87].

# Erster Townsend-Koeffizient

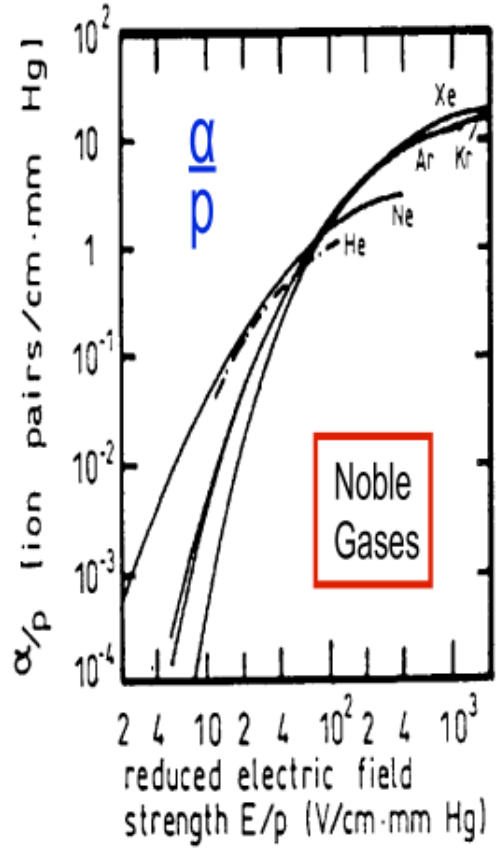


Fig. 4.7. First Townsend coefficient for some noble gases [51, 143, 144, 145].

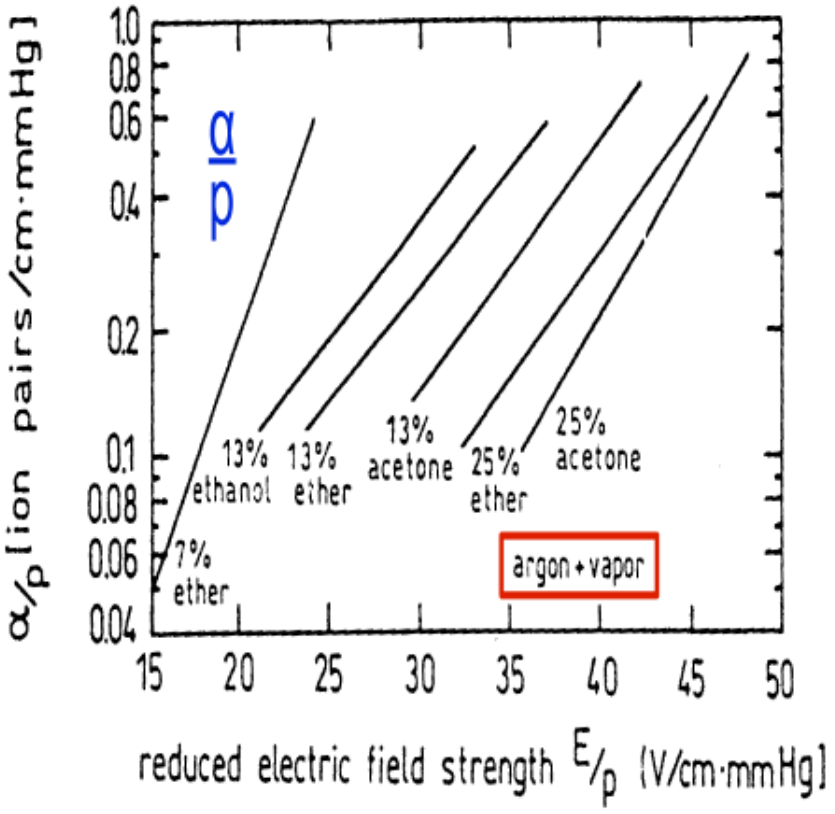


Fig. 4.8. First Townsend coefficient for argon with some organic vapor admixtures [51, 146, 147].

Time development of the avalanche:

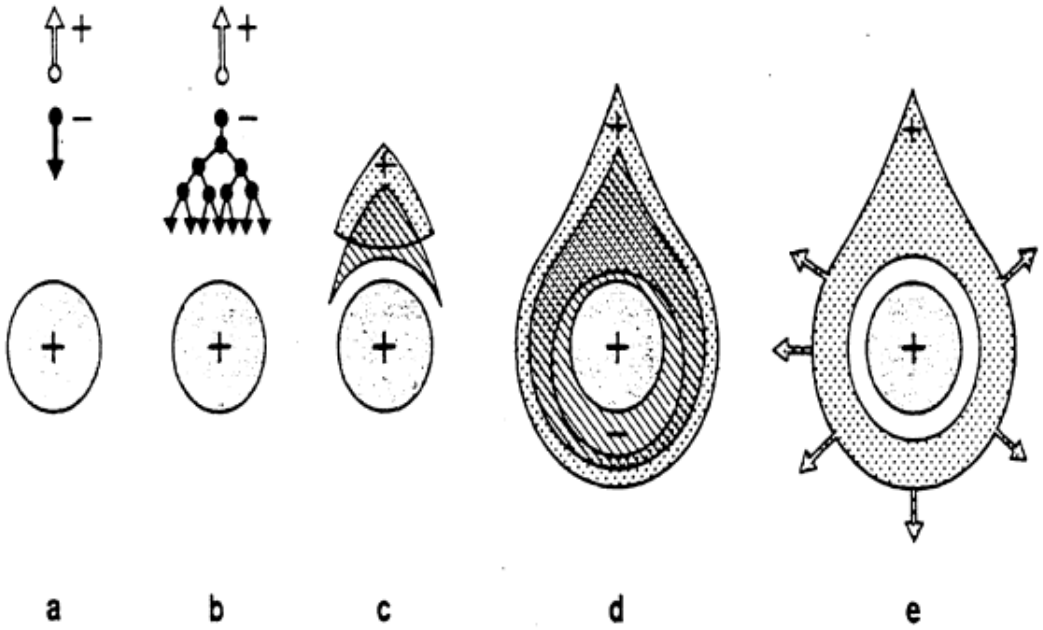


From: F. Sauli, „Principles of Operation of Multiwire Proportional and Drift Chambers“, CERN-77-09

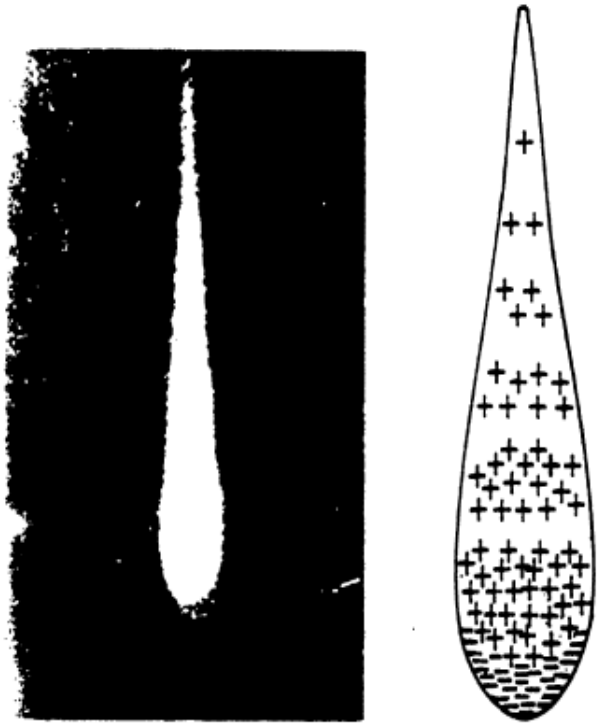

Fig. 46 Drop-like shape of an avalanche, showing the positive ions left behind the fast electron front. The photograph shows the actual avalanche shape, as made visible in a cloud chamber by droplets condensing around ions[18].

# Proportionalzählrohr: Differentation des Signal

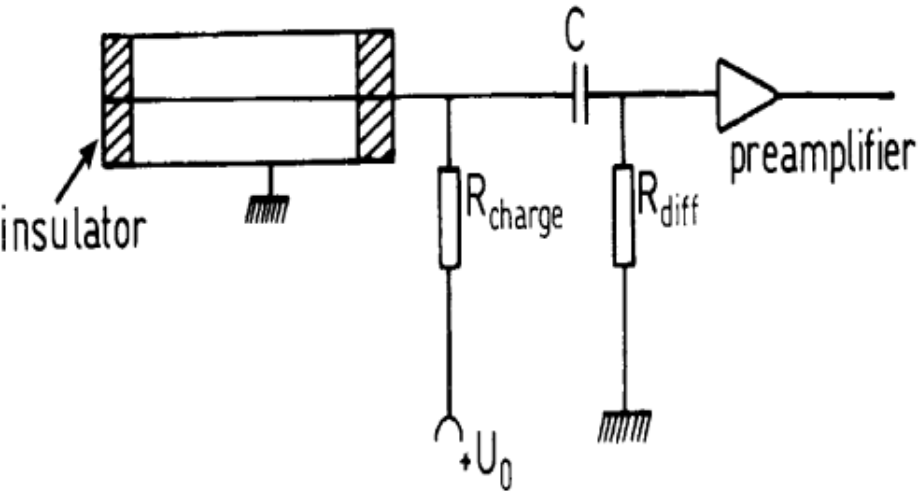


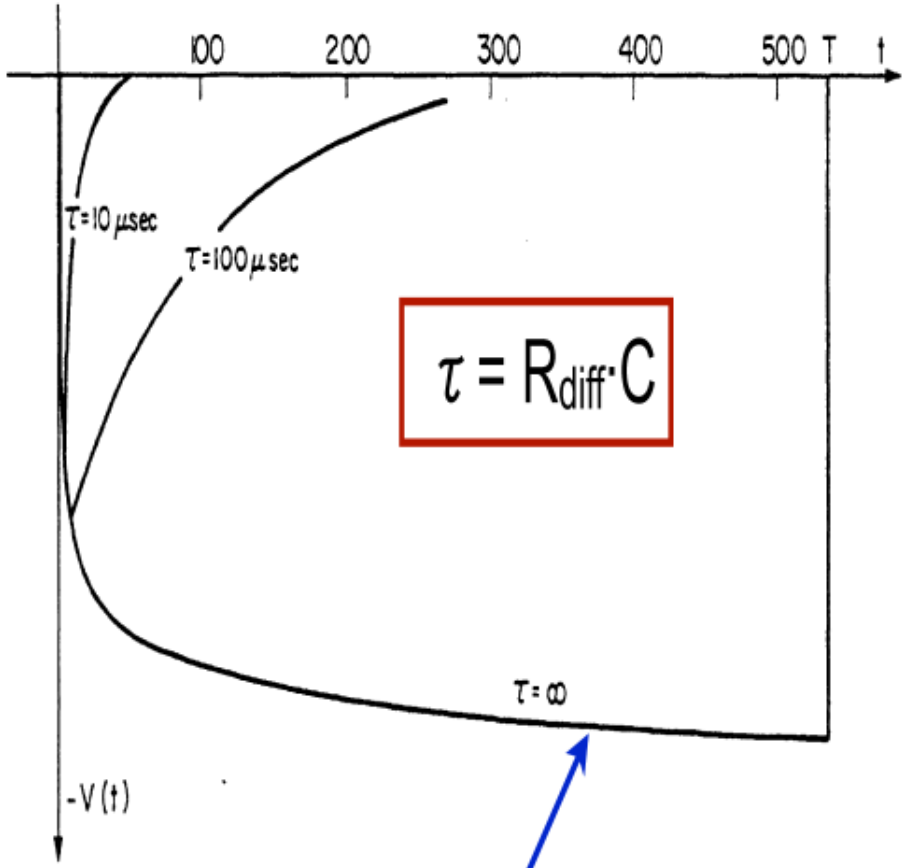


calculated from positive ions only

# Lawinenbildung im Geiger-Modus ohne Löschung

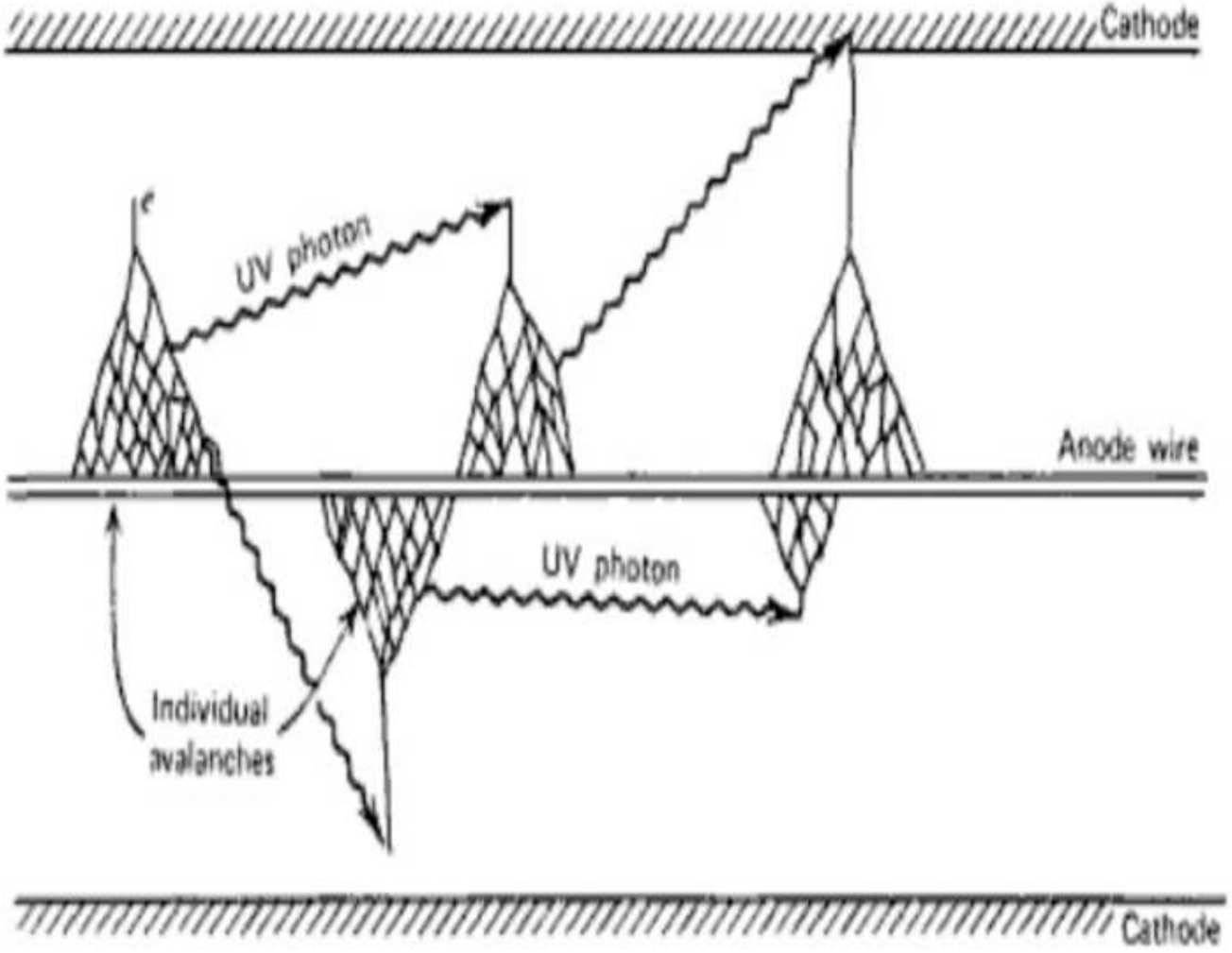


**Figure 7.1** The mechanism by which additional avalanches are triggered in a Geiger discharge.

# Lawinenbildung in verschieden Betriebsbereichen

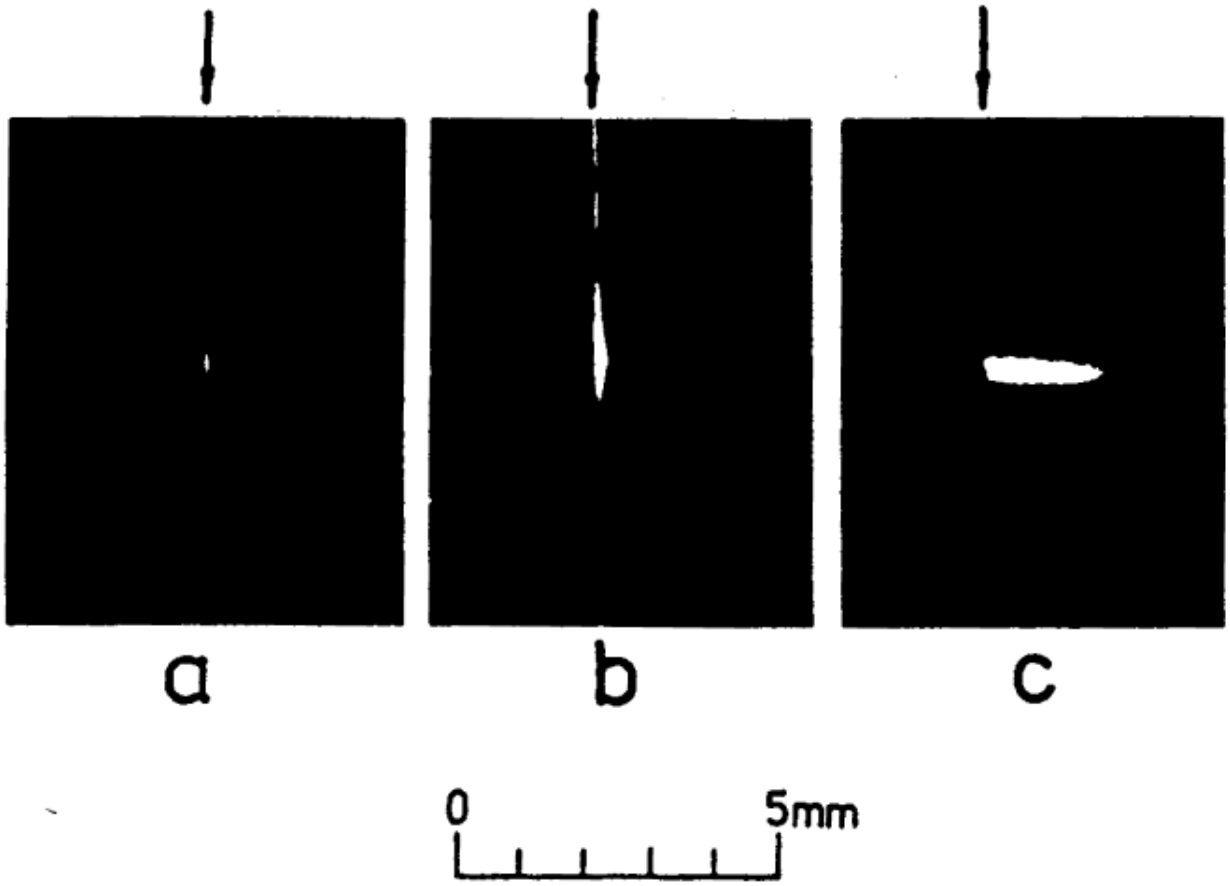


**Fig. 4.17.** Gas discharges in (a) a proportional counter, (b) a Geiger counter, and (c) a self-quenching streamer tube; the arrows indicate the position of the anode wire [166].

# Lawinenbildung in verschieden Bereichen

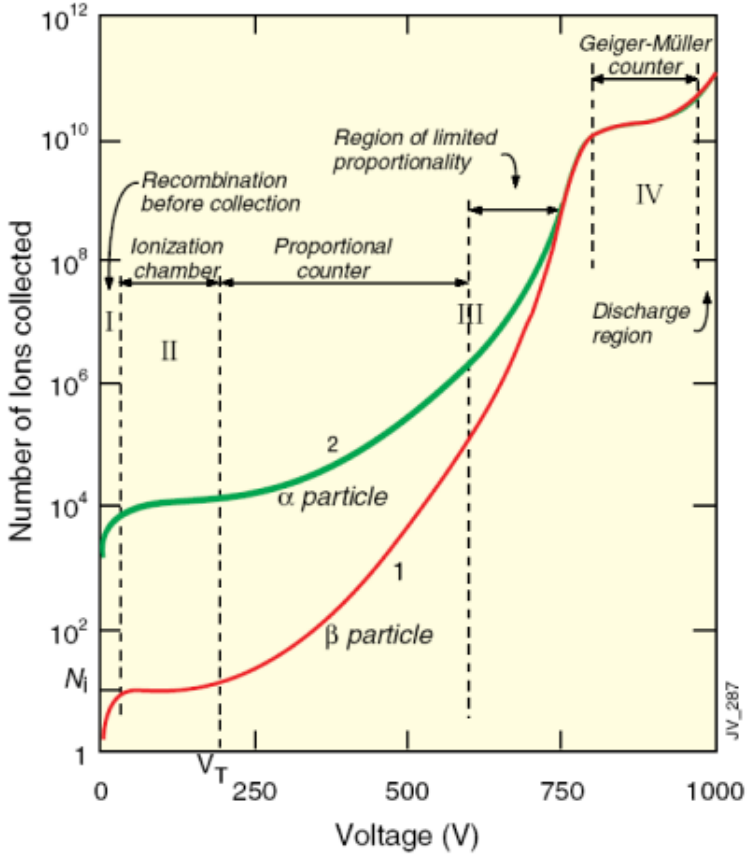


Ionization Chamber:
All charge collected, but no charge multiplication

Proportional Chamber:
Gas amplification
Signal ~ primary ionization
Typical gain $10^4$ - $10^5$

Limited proportional mode (streamer mode):
Secondary avalanches merging with primary avalanche
Typical gain $10^{10}$ → Large signals (simple electronics)

- Geiger-Müller Counter:
  Secondary avalanches over the full anode wire
  Discharge stopped by cutting HV

# Betriebsarten von Ionisationskammern

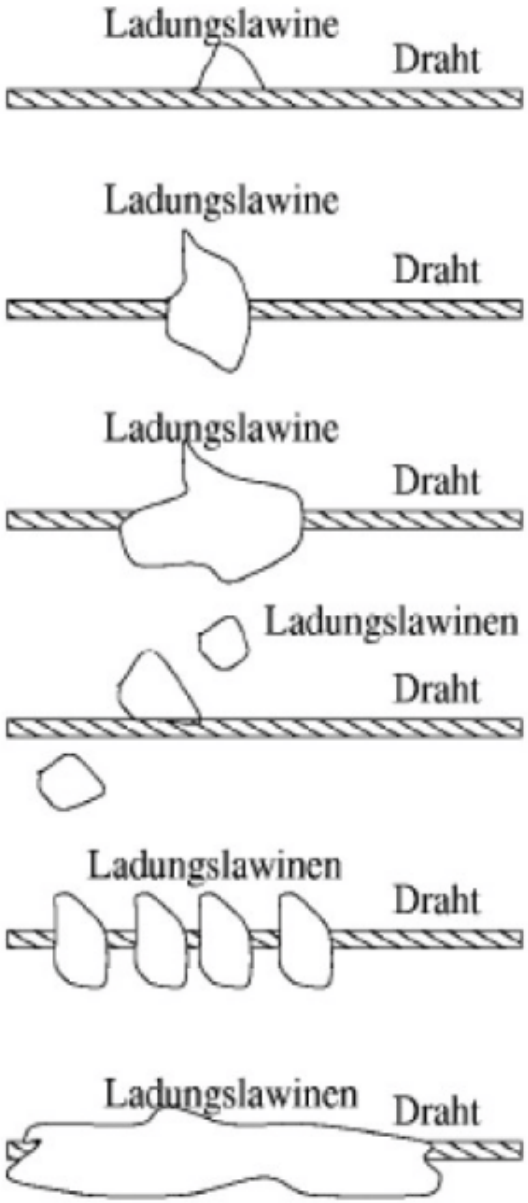


- Ionization Chamber:
  All charge collected, but no charge multiplication

- Proportional Chamber:
  Gas amplification
  Signal ~ primary ionization
  Typical gain $10^4$ – $10^5$

- Limited proportional mode (streamer mode):
  Secondary avalanches merging with primary avalanche
  Typical gain $10^{10}$ → Large signals (simple electronics)

- Geiger-Müller Counter:
  Secondary avalanches over the full anode wire
  Discharge stopped by cutting HV

# Vieldrahtproportionalkammer (1968)

G. Charpak
(Nobel Prize 1992)

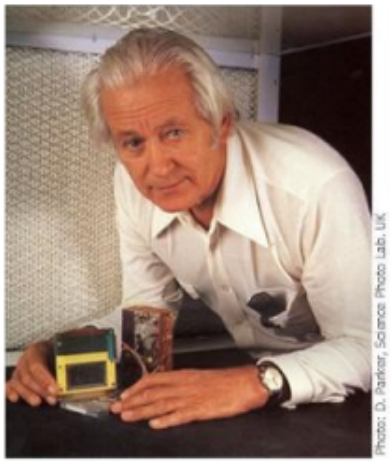


Principle: Put many anode wires in parallel, in one volume

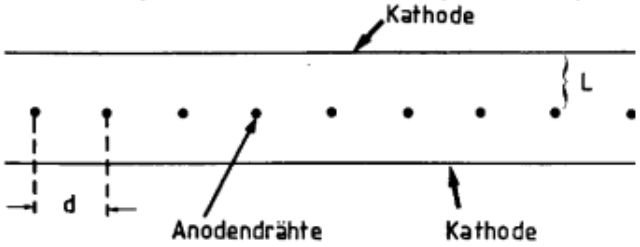


- Every wire acts as an independent proportional tube

  → every anode wire is read out separately
  → space information

- Typical parameters:
  distance between wires: d = 2 mm
  distance anode-cathode: L = 7-8 mm
  diameter of anode wires: 10 – 30 μm

- Achievable coordinate resolution:
  $\sigma = d / \sqrt{12} \sim 600\ \mu m$

# Aufbau und Feldkonfiguration in MWPC

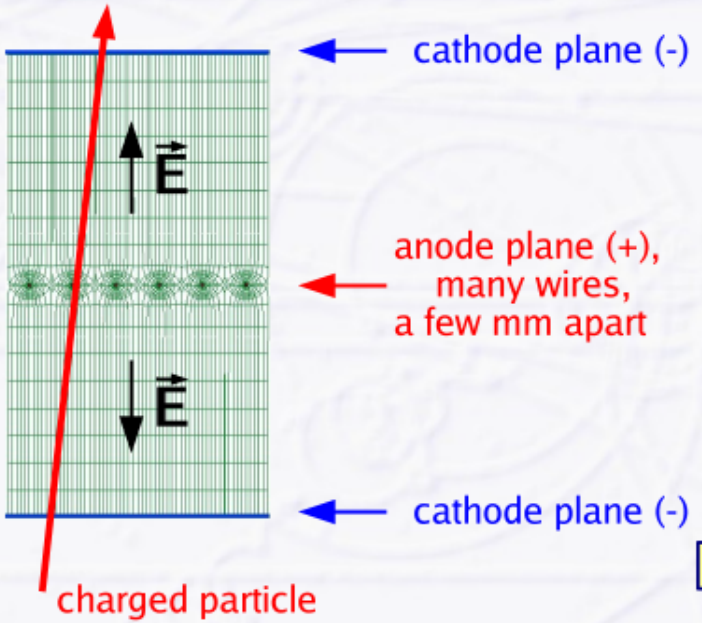



Georges Charpak, Fabio Sauli and Jean-Claude Santiard

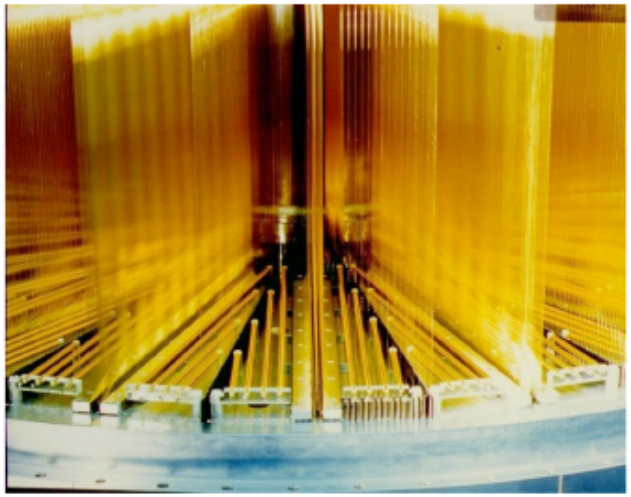

# Aufbau und Feldkonfiguration in MWPC

Multiple signal wires with common cathodes:

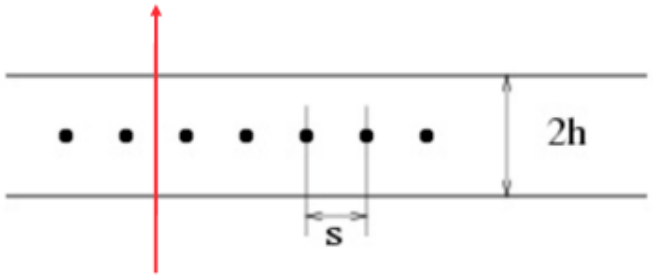


Wire diameters: 10µm - 50µm
Wire distance: typ. 2mm
Wire-Cathode distance: typ. 10 mm

Field in multiplication region still symmetric

Field outside multiplication region approx. const.

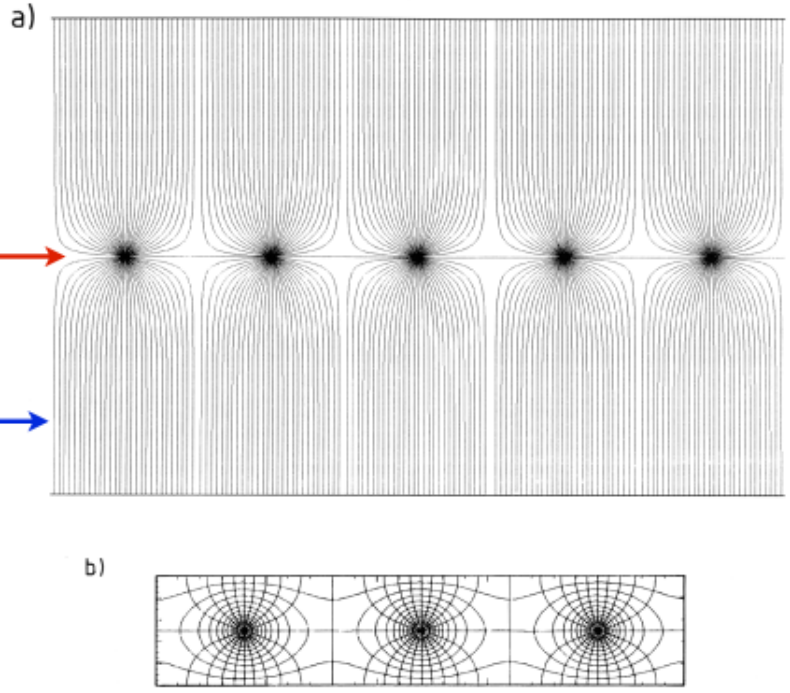


Fig. 4.25. a) Field lines in a five-wire proportional chamber [184]. b) Field and equipotential lines in a three-wire proportional chamber [183].

# MWPC: (x,y)-Ortskoordinaten mit Kathodenauslese

- Segment cathode plane → strips
- Ions induce positive signal on cathode strips
- Readout cathode signal → second coordinate
  improvement of resolution

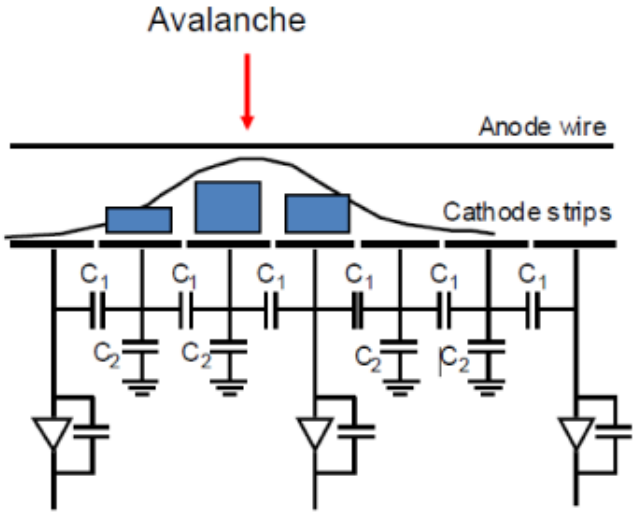


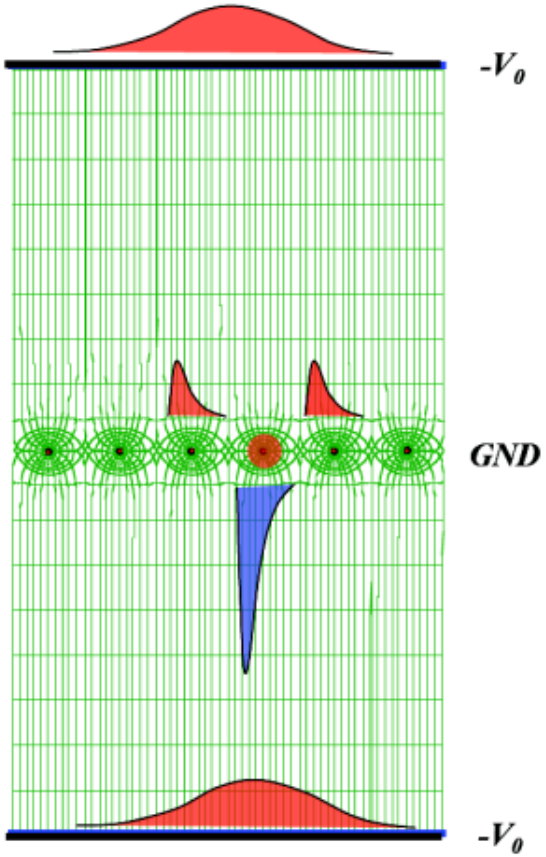


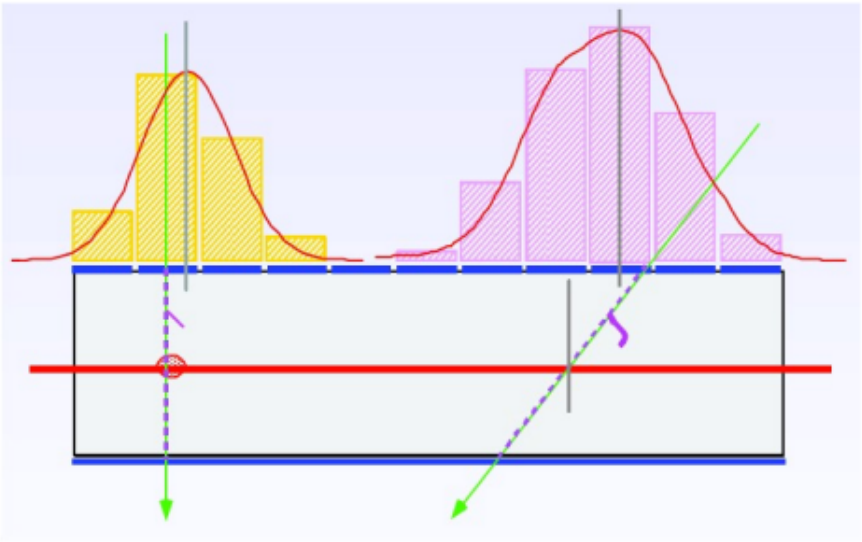

signal distributed over several strips

# MWPC: (x,y)-Ortskoordinaten mit Kathodenauslese

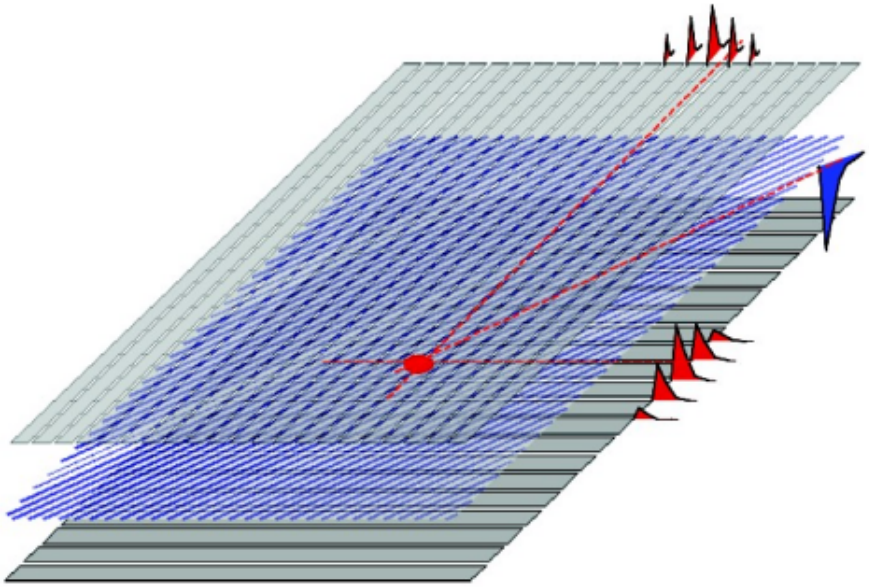

e.g. cathode strips perpendicular in upper/lower plane

Coordinate by centre of gravity:

$$X = \sum \frac{X_i \, A_i(X)}{A(X)} \qquad Y = \sum \frac{Y_i \, A_i(Y)}{A(Y)}$$

Typical resolution 50-100 µm

Solving multi-particle ambiguities:

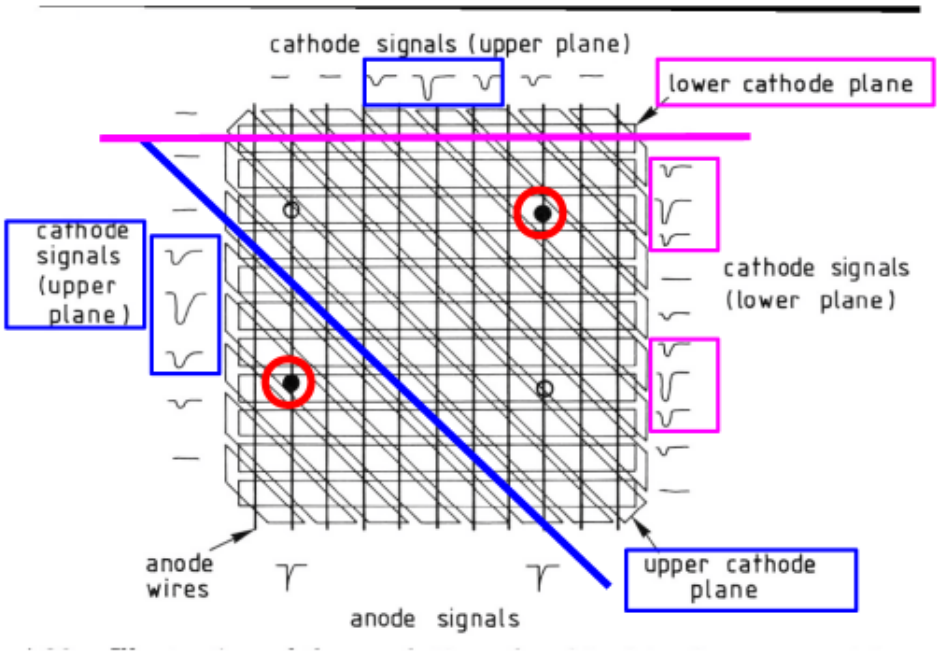

# MWPC: Bestimmung mehrerer Ortskoordinaten

Application of MWPC in a typical (fixed target) experiment:

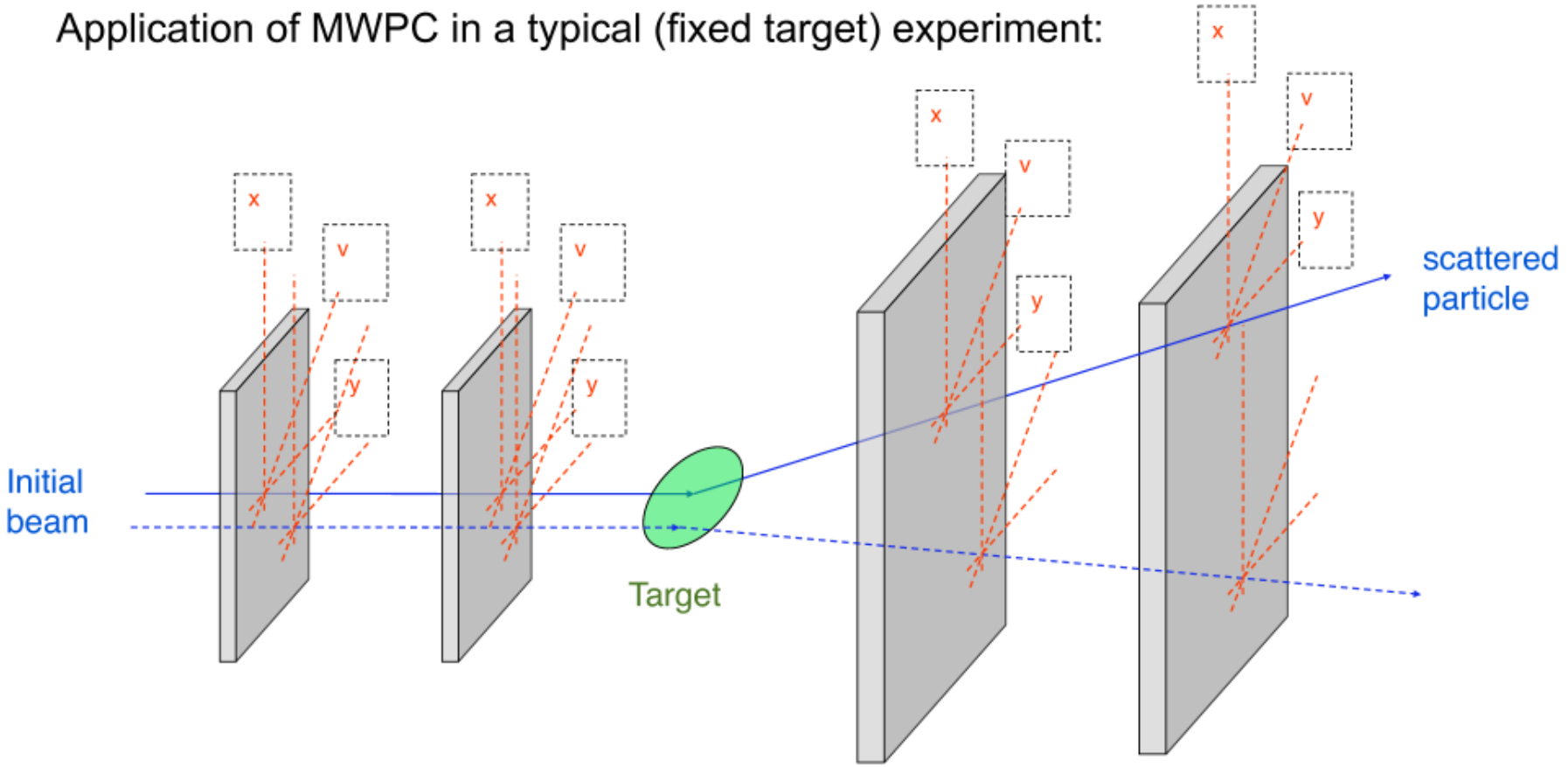


Many planes with different orientations, single plane precision ≈ 1 mm, event rates up to 100 kHz